Journal Pre-proof

A tool for solving bone growth related problems using finite elements adaptive meshes

M.G. Alonso, A. Yawny, G. Bertolino

PII: S1751-6161(21)00577-4
DOI: https://doi.org/10.1016/j.jmbbm.2021.104946
Reference: JMBBM 104946

To appear in: *Journal of the Mechanical Behavior of Biomedical Materials*

Received date : 21 July 2021
Revised date : 17 September 2021
Accepted date : 26 October 2021

Please cite this article as: M.G. Alonso, A. Yawny and G. Bertolino, A tool for solving bone growth related problems using finite elements adaptive meshes. *Journal of the Mechanical Behavior of Biomedical Materials* (2021), doi: https://doi.org/10.1016/j.jmbbm.2021.104946.

A tool for solving bone growth related problems using finite elements adaptive meshes.

M. G. Alonso[a,b,c,*], A. Yawny[a,b,c], G. Bertolino[a,b,c]

[a] *División Física de Metales, Centro Atómico Bariloche, CNEA, (8400) Bariloche, Argentina*
[b] *CONICET*
[c] *Universidad Nacional de Cuyo, Instituto Balseiro*

Abstract

Long bones geometry changes in response to longitudinal growth in the epiphyseal plates and hydroxyapatite apposition in the periosteum. Due to its relevance for growth modulation and orthotics performance, researchers have extensively modeled these phenomena, using the finite elements method for it almost since the introduction of modern computers. This is a rather complex task that, besides the inherent difficulty of solving the models equations, requires considering a moving boundary. Here, the development of a new computational tool for its resolution is described. A generalized formulation of these problems is established based on the most common approaches taken in the literature and a novel finite elements algorithm is proposed for its resolution. The later allows a significant reduction of the spatial discretization requirements, the computational cost and the numerical errors associated with more classical approaches. The potentiality of the method is demonstrated by its application to three cases of practical interest, namely, hemiepiphysiodesis treatment, growth in the distal femur and bone remodeling around hip prosthesis. Eight relevant cases of study and an open source implementation of the proposed algorithm are also provided as supplementary material.

Keywords: Mechanobiology, Moving boundary, FEM, Bone, prosthetic

* Corresponding author
Email address: marcelo.alonso@cab.cnea.gov.ar (M. G. Alonso)

1. Introduction

Shape and function of long bones is the result of a series of processes that occur during the whole life of vertebrates [1]. The involved mechanisms are often referred to as endochondral growth and ossification . [2, 3] During childhood and adolescence, growth and ossification of cells located in the epiphyseal plate are the main causes of what is called longitudinal growth [4]. Osteoclasts and osteoblasts act by modifying the amounts of hydroxyapatite on the bony tissue, thus changing its shape and density [5, 6]. This particular process is called bone remodeling.

All these phenomena respond to a wide variety of factors, as hormonal activity [7, 8, 9], drug treatments [10] or mechanical loads [11, 12]. Researchers have extensively studied endochondral growth given its fundamental role in the development of growth pathologies [13]. Bone remodeling also plays an important role in the development of pathologies as osteoporosis [14], as well as in the performance of bone implants and orthotics [15, 16].

Multiple authors have numerically modeled these phenomena by using the finite elements method (FEM). One of the firsts applications of the FEM for studying bone growth and ossification was made by Carter and Wong [17], who analyzed the effect of mechanical loads on the development of diarthrodial joints. Stokes and Laible [18] studied bone longitudinal growth for a 3D model of a rib cage composed of 1D elements in an attempt to gain insight into idiopathic scoliosis causes. Carter et al. [19], and Orr and Beaupré [15] also studied bone internal remodeling as well as bone growth and ossification, based on phenomenological observations. More complex phenomenological models have been recently applied to study the origin of spine deviations [20], the development of diarthrodial joints [21, 12], longitudinal growth in the femur [22], and bone external as well as internal remodeling [23]. Also, progress in research of the sub laying biochemical mechanisms responsible for growth has led to application of the FEM to study drug [10] and hormonal [9] effects on bone morphology.

In the literature, growth is frequently modeled by neglecting remodeling, considering the bone structure as formed by constant properties, differentiated tissue regions. This is usually achieved by partitioning the used mesh in two sets of "growing" and "non growing" elements. Geometry evolution is described by a growth rate tensor $\dot{\varepsilon}_{ij}$, that depends on the stress state of the tissue at a given time t. Growth is computed following a step-wise algorithm, for which geometry is modified in response to an increment in bone growth tensor given by:

$$\Delta\varepsilon_{ij} = \dot{\varepsilon}_{ij}\Delta t, \tag{1}$$

with a pre-defined time step Δt. This numerical scheme is usually implemented trough the thermal expansion capabilities of the used solver, to allow expansion of the considered geometry using this step increment as the "temperature" for expansion. The new geometry is updated, and mechanically induced stresses are re-computed for the next step. Elements that following some modeling criteria are considered to ossify are assigned to the non growing region, while the remaining elements are used for computing growth in the next step.

This numerical approach has been successfully used in modeling several cases [7, 24, 25, 21, 22]. Nevertheless, it is not free of complications, specially due to the used meshes variations in time. These issues are of different nature, depending on the considered problem.

When studying endochondral growth and ossification, as the bone rudiments consist of a cartilaginous matrix in which chondrocytes distribution is random and isotropic, growth is analogous to an isotropic volumetric expansion. For these cases, Eq. 1 yields an increase in size of the "growing" region, Fig. 1. This results in an increase of elements characteristic length L_c, causing a reduction in the spatial resolution of the model. This has two relevant numerical effects: an increase of interpolation errors for the computed space-dependent model quantities, and an increased uncertainty on the ossified and cartilaginous zones determination. Even though interpolation errors can be reduced by remeshing the domain to keep L_c approximately constant when time advances,

as implemented by Giorgi et al. [21], errors in the determination of the ossified interface position (non-growing) and the cartilaginous (growing) zones cannot be reduced beyond L_c.

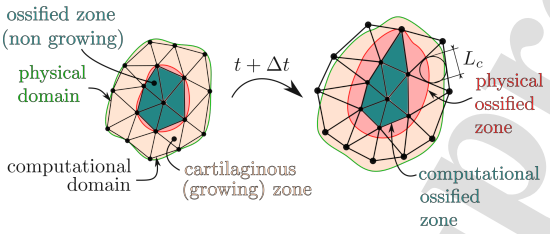

Figure 1: Discretization errors that arise when solving endochondral growth and ossification problems. Uncertainty in the position of the ossified zone interface cannot be reduced beyond the elements characteristic length L_c.

These numerical issues do not invalidate results when modeling situations in which mesh does not undergo large deformations, as studied by Beaupré et al. [26], or when ossification is not considered, as modeled by Giorgi et al. [21]. Nevertheless, when modeling longitudinal growth this poses a great challenge. Due to the highly anisotropic histological structure of the epiphyseal plate, growth proceeds mainly along a preferential direction [27, 22]. Also, in the long bones, longitudinal growth can represent in the order of 3 to 6 times the epiphyseal plate height e [28, 29] for a period of time in the order of a year, of relevance to study some growth pathologies [13, 30]. Computational consequences of this are showed in Fig. 2, for a linear growth situation as studied by Alonso et al. [31] or Mikic [7]. Being the epiphyseal plate a thin structure, in order to reduce computational cost, its height is usually subdivided in a reduced number of elements of characteristic length L_c [24, 20, 22]. For long simulation times, two situations may arise, depending on whether the adopted time step is larger or smaller than a characteristic time t'. For a small time step, simulation proceeds as indicated in the green curve of Fig. 2. The adopted spatial discretization causes the elements in the epiphyseal plate to undergo an elongation that increases the computational epiphyseal height e', Fig. 2 (d). This

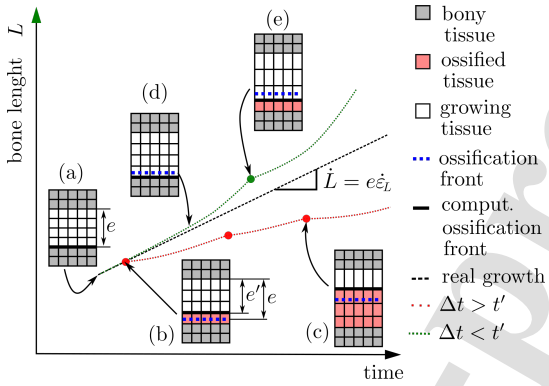

Figure 2: Discretization errors that arise when solving longitudinal growth and ossification problems with the algorithms more frequently applied in the literature.

redounds in a corresponding increase of the computed growth speed. A delay in the advance of computational ossification front occurs, as compared with the physical ossification front. This causes computed length to exponentially grow, with a corresponding elongation of the used mesh, Fig. 2 (e). For time steps bigger than the characteristic time t', computational ossification front advance is accelerated as compared with the physical ossification front. This causes the computational epiphyseal height e' to reduce as the simulation proceeds (b), until all elements in the mesh are ossified and no further time advance can be computed, as shown by the red curve in Fig. 2.

The above described alterations in the computed epiphyseal height are not consistent with the underlying biology of the problem. They are caused both for the method used to represent cartilage ossification and having a finite amount of elements representing the epiphyseal plate. Furthermore, as elements deformation for these cases is highly anisotropic, errors due to the resulting poor elements shape factor are caused. Although it would be theoretically possible to reduce these errors by remeshing the geometry and refining mesh in the vicinity of the ossification front, this can be done only with an increase of computational cost. This constricts the applicability of the described algorithm to the study

of cases in which small elements elongation is produced [24], or relatively small time intervals are considered [22].

In the present work, we focus on the numerical resolution of a general formulation of bone growth and remodeling problems, based in the method initially proposed by Beaupré et al. [26]. We present a novel algorithm that is able to overcome the previously described modeling difficulties that arise when computing bone growth. In particular, the manner in which we solved the tracking of the moving boundary between the cartilaginous and the ossified regions allows the precise resolution of a wide variety of problems, and this could be a valuable asset for research purposes. In what follows we focus on the description of the applied resolution techniques, as well as on the demonstration of the proposed algorithm capabilities. For the later we have chosen three practical interest cases. Code validation as well as a set of additional implementation examples are provided in a supplementary material.

2. Methods

2.1. Mathematical problem posing

In the present work, we consider a macroscopic and continuous description of bone growth and remodeling, that consists of:

- Finding the spatial evolution of a bone or a bone/prosthesis system described by a domain $\Omega \subset \mathbb{R}^N$ ($N \leq 3$). A set of k pairs load-cycles number $\{f_i, n_i\}$ is prescribed, and for each of these, its boundary $\partial\Omega$ is partitioned in an essential $\partial\Omega_D^{(i)}$ and a natural $\partial\Omega_N^{(i)}$ region, such that $\partial\Omega = \partial\Omega_N^{(i)} \cup \partial\Omega_D^{(i)} \wedge \partial\Omega_N^{(i)} \cap \partial\Omega_D^{(i)} = \varnothing$, defining what we call a load state. For each load state, equilibrium condition are given by:

$$\begin{cases} \nabla \cdot \sigma^{(i)} + b_i & = 0 \text{ in } \Omega \\ \sigma^{(i)} \cdot \hat{n} & = f_i \text{ in } \partial\Omega_N^{(i)} \\ u & = \overline{u}_i \text{ in } \partial\Omega_D^{(i)}, \end{cases} \tag{2}$$

being $\sigma^{(i)}$ the Cauchy stress tensor for the ith load, b_i the volumetric forces acting on the bone, u the displacement vector and $\hat{n}$ the normal to $\partial\Omega$. A set of essential boundary conditions is prescribed in a subset $\partial\Omega_D^c \subseteq \partial\Omega$, limiting the domain growing displacements. For simplicity, we will call $\partial\Omega'_N$ at the subset of $\partial\Omega_N$ for which $f_i \neq \vec{0}$. Alternatively, this load cases based description could be replaced by a single set of loads $f(t)$ defined on a region $\partial\Omega_N$, along with a set of prescribed displacements in an essential boundary $\partial\Omega_D$. It must be noticed that elastic properties might not be continuous Ω, and singularities may appear in the solution of Eqs. 2.

- Determining the evolution of a maturity function $M(\vec{r},t) \rightarrow \mathbb{R}^+$, for $\vec{r} \in \Omega$, describing tissue differentiation and age. This function is such that values of $M(\vec{r},t) = 0$ represent cartilaginous zones of newborn chondrocytes, and values of $M(\vec{r},t) \geq 1$ are associated with ossified zones. Two subsets Ω_B and Ω_F that we will further refer as bony region and growing region respectively, such that $\Omega_B \cup \Omega_F \subset \Omega \wedge \Omega_B \cap \Omega_F = (\Omega_B \cup \Omega_F) - (\text{int}(\Omega_B) \cup \text{int}(\Omega_F)) \wedge \Omega_F = \{\vec{r} \in \Omega / M(\vec{r},t) \leq 1\}$ are defined. We require the Hessian matrix $\mathscr{H}_M(\vec{r},t)$ of function $M(\vec{r},t)$ to be such that $\mathscr{H}_M(\vec{r},t) \neq 0, \forall \vec{r} \in int(\Omega_F)$. Alternatively, a third partition $\Omega_P \subset \Omega$ can be defined.

- Determining the bone apparent density evolution $\rho(\vec{r},t)$ for each $\vec{r} \in \Omega$.

The problem description is complete once a set of phenomenological as well as material governing equations and initial conditions are defined. Initial conditions are given by the bone shape $\Omega(0) = \Omega_0$, stress $\sigma(\vec{r},0) = \sigma_0(\vec{r})$, maturity $M(\vec{r},0) = M_0(\vec{r})$, and density $\rho(\vec{r},0) = \rho_0(\vec{r})$.

Material governing equations comprise the laws that describe the material behavior and the tissue specific correlations between elastic properties and apparent density. We will consider only linear-elastic materials, thus reducing governing equations to one. A tensor $\mathbf{E}(\rho, M, \vec{r}, t)$ describing bone mechanical behavior is defined, in such a manner that stress and strain are related by:

$$\sigma = \mathbf{E}\varepsilon. \tag{3}$$

Phenomenological equations describe the bone rate of growth, maturation and remodeling. These equations can be based on empirical observations or biochemical models. Empirical equations describe the aforementioned rates of change in terms of explicit functions of the stress or strain to which bone is subjected [26, 23, 32]. Biochemically based equations are obtained after considering these changes as the result of a series of chemical processes, regulated by the influence of stress or strain on growth factors concentrations [9, 10]. Considering these observations, a bone growth and remodeling problem is completely defined once the following parameters are defined:

- A maturation rate function,

$$\dot{M}(\vec{r},t) = g(M,\sigma_1,...,\sigma_k,n_1,...,n_k,\mathbf{E},t). \tag{4}$$

- A potential growth velocity tensor,

$$\begin{aligned} \dot{\varepsilon}_{ij}(\vec{r},t) &= f(M,\sigma_1,...,\sigma_k,n_1,...,n_k,\mathbf{E},t) &(5)\\ &= \frac{1}{2}[\partial_j \dot{u}_i(\vec{r},t) + \partial_i \dot{u}_j(\vec{r},t)], &(6)\end{aligned}$$

  being $u_{i,j}$ the displacements along directions i,j due to growth only of a point of coordinates $\vec{r} \in \Omega_F$ at time t.

- A rate of hydroxyapatite apposition/deposition,

$$\dot{r}(\vec{r},t) = \dot{r}(M,\sigma_1,...,\sigma_k,n_1,...,n_k,\mathbf{E},\rho,t). \tag{7}$$

  For $\vec{r} \in \text{int } \Omega_B$, this function depends with bone density rate of change by an empirical factor $S_v(\rho)$ representing the bone surface area density, and a factor ρ_a that represents the density of the deposited bone, i. e.:

$$\dot{\rho}(\vec{r},t) = \rho_a S_v(\rho)\dot{r}(\vec{r},t). \tag{8}$$

  The rate of bone apposition/removal relates with the displacement velocity in the border of the bony region $\partial\Omega_B$ by:

$$\dot{u}(\vec{r},t) = \dot{r}(M,\sigma_1,...,\sigma_k,n_1,...,n_k,\mathbf{E},\rho,t)\hat{n}, \tag{9}$$

  being $\hat{n}$ the normal to the surface $\partial\Omega_B$.

2.2. Proposed algorithm

The algorithm that we propose on this work can be divided in seven steps:

1. **Initialization:** An initial density distribution $\rho_0(\vec{r})$ is defined for each node of Ω_B. Elastic properties are defined for each element in the model, by interpolating the function $\rho_0(\vec{r}, t)$ onto the Gauss integration points of the finite elements mesh. An initial maturity distribution $M(\vec{r})$ is defined as a nodal quantity. A growth due stress is defined, as a Cauchy tensor $\sigma(\vec{r}, t)$, for every element in the model. This tensor is initialized as $\sigma(\vec{r}, t) = \sigma_0(\vec{r})$.
2. **Loading stresses determination:** Problem defined in Eq. 2 is solved for each of the defined load states. For this, stiffness matrix of the model is calculated, and the usual finite elements approach is used. Stress tensor is computed for each element of the model, and for each of the load states.
3. **Growth displacements computation:** A growth velocity tensor $\dot{\varepsilon}^{(e)}$ (Eq. 5) is computed for each element in Ω_F with the stresses obtained in step 2. A growth increment tensor $\Delta\varepsilon^{(e)}$ is computed as,

$$\Delta\varepsilon^{(e)} = \dot{\varepsilon}^{(e)}\Delta t. \tag{10}$$

A set of growth nodal forces is calculated for each element, as:

$$f_i^{(e)} = \int_V \boldsymbol{B}^t \boldsymbol{D} \Delta\varepsilon^{(e)} dV, \tag{11}$$

being $\boldsymbol{B}$ and $\boldsymbol{D}$ the displacements differentiation and Hook matrices of the elements respectively. This nodal forces, as well as the essential boundary conditions for $\partial\Omega_D^c$ are applied, as usual, to obtain the nodal displacements due to growth, i. e.,

$$u_i^c = \boldsymbol{K}^{-1} f_i, \tag{12}$$

being $\boldsymbol{K}$ the stiffness matrix of the system. Growth stress tensor $\sigma^{(e)}(\vec{r}, t)$ is updated for each element, as:

$$\sigma^{(e)}(t + \Delta t) = \sigma^{(e)}(t) + \boldsymbol{D}\boldsymbol{B}_j u_j^c - \boldsymbol{D}\Delta\varepsilon^{(e)}. \tag{13}$$

4. **Tissue differentiation and mesh adaptation:** For each node in Ω_F, maturation rate $\dot{M}_i$ (Eq. 4) is computed. For this, stresses obtained in step 2 are projected into the mesh nodes by using the elementary shape functions. An auxiliary nodal maturity M_i' is computed, as:

$$M_i' = M_i + \dot{M}_i \Delta t + \nabla M_i u_i^c. \tag{14}$$

Here, ∇M_i is the maturity gradient, and u_i^c the displacements computed in step 3. For each element (e), this gradient is obtained from the elementary shape functions derivative, and then projected again to the elements nodes. Mesh adaptation is performed by moving the nodes of Ω_F, for which $M_i \geq 0$, in such a manner that these 'follow' the points of the space that have the same maturity as initially defined in step 1. In order to produce a minimal mesh distortion, in terms of deviations from the initial mesh, nodal displacements $\tilde{u}_i$ are computed as:

$$\tilde{u}_i = k \nabla M_i. \tag{15}$$

This condition implies that, as nodes are moved along the direction of maximum change in maturity function $M(\vec{r}, t)$, $|\tilde{u}_i|$ is minimal. Requiring the nodes to be always at a point having the same maturity as initially assigned can be expressed, at the first order, as:

$$M_i' + \nabla M_i \cdot \tilde{u}_i = M_i, \tag{16}$$

which implies that

$$k = \frac{M_i' - M_i}{|\nabla M_i|^2}. \tag{17}$$

5. **Geometry updating:** Mesh geometry is updated by applying a displacement v_i to each node in Ω, being

$$v_i = u_i^c + \tilde{u}_i. \tag{18}$$

6. **Bone remodeling computation:** Remodeling rate $\dot{r}$, Eq. 7, is computed using stresses obtained in step 2. Normal vector $\hat{n}$ is computed for

the elements in $\partial\Omega_B$. A nodal displacement $\tilde{u}_i^r$ is defined according to Eq. 9. For nodes in int Ω_B, $\tilde{u}_i^r = 0$. Geometry is updated by displacing each node in the model by $\tilde{u}_i^r$. Density distribution ρ_i is updated as

$$\rho_i(t + \Delta t) = \rho_i(t) + \rho_a S_v(\rho)\dot{r}_i + \nabla\rho_i \tilde{u}_i^r, \tag{19}$$

being $\nabla\rho_i$ the density gradient, computed in the same fashion as maturity gradient in step 4.

7. **Re-initialization:** Elastic properties tensor is updated for each element in the model. If a prescribed condition is fulfilled, domain Ω_B is re meshed, and all the defined fields are projected into the new mesh. Algorithm is repeated from step 2, until reaching a stopping condition.

3. Results

The proposed algorithm has been implemented as a Cast3M [33] package, which is provided as Supplementary Material N° 1, and allows the study of several cases of bone growth and/or bone remodeling problems. The examples we show here, as well as a set of 3 code-validation cases, and 3 implementation examples of classical problems are also incorporated on the mentioned supplementary material. The provided code has been implemented in such a manner that a user familiarized with Cast3M can straightforwardly modify the growth and/or the bone remodeling equations. We have defined a default set of growth and remodeling equations, based on the more frequently referenced models available in the literature. These are specified in Sec. 3.1.

A set of three practical interest examples has been chosen to illustrate the capabilities of the proposed algorithm. We begin with a 2D model of the distal femur under an hemiepiphysiodesis treatment. We continue by demonstrating how biomechanical data can be considered with a 3D finite elements contact model to compute bone growth and remodeling in the distal femur, and finish showing how a classical 3D remodeling problem around a hip prosthesis can be solved. Geometrical models shown here were obtained from the Standardized

Femur [34], and the Cal Poly Human Motion Biomechanics Lab Knee Joint Finite Element Model [35] with Salome-Mesh [36].

3.1. Example model equations

Bone growth:. Growth speed velocity tensor is computed in a similar way as proposed by Beaupré et al. [6] and other authors [12, 20]:

$$\dot{\varepsilon}_{ij} = (\dot{\varepsilon}_M + \dot{\varepsilon}_B)\varepsilon_{ij}. \tag{20}$$

being ε_{ij} the tensor defined by $\varepsilon_{ij} = 1$ and $\varepsilon_{ij} = 0$ if $i, j \neq 2$ for $2D$ cases, and $\varepsilon_{ij} = 1$ if $i = j = 3$ and $\varepsilon_{ij} = 0$ otherwise, for 3D cases. $\dot{\varepsilon}_B$ represents the bone biological growth speed, and was defined as $\dot{\varepsilon}_B = 3$ year^{-1}, as it can be derived for a person in the peak of growth [28], for a typical growth thickness [37]. For the mechanical stimulus to growth, $\dot{\varepsilon}_M$ was computed as:

$$\dot{\varepsilon}_M = \kappa_M \sum_{i=1}^{k} n_i \sigma_{hi}, \tag{21}$$

being σ_{hi} the hydrostatic stress for the i-th load state, n_i the number of load cycles and κ_M a constant, here set as 1×10^{-4} MPa^{-1}month^{-1}. $\dot{\varepsilon}_M$ is truncated, in such a manner that for every point in Ω_F, $-\dot{\varepsilon}_B \leq \dot{\varepsilon}_M \leq \dot{\varepsilon}_B$.

Maturation speed, Eq. 4, is computed as:

$$\dot{M}(\vec{r}, t) = \sum_i \dot{\varepsilon}_{ii}(\vec{r}, t), \tag{22}$$

for every $\vec{r} \in \Omega_F$ and $\dot{M}(\vec{r}, t) = 1$ for every $\vec{r} \in \Omega_B$.

Bone remodeling:. As default case, for points $\vec{r} \in \Omega_B$, bone apposition rate is computed as suggested by Beaupré et al. [26], i. e.:

$$\dot{r}(\vec{r}, t) = \dot{r}_B(\vec{r}, t) + \dot{r}_M(\vec{r}, t), \tag{23}$$

being $\dot{r}_B$ a biological and $\dot{r}_M$ a mechanical contribution to bone apposition. Biological contribution is computed as $\dot{r}_B = \exp[-k_r(M - 1)]$. By default, a value of $k_r \to \infty$ is set.

Mechanobiological contribution to bone apposition is given by

$$\dot{r}_M = \begin{cases} C_{in}[S-(1+s)S_{ref}], & \frac{S}{S_{ref}} > (1+s) \\ 0, & -s < \frac{S}{S_{ref}} - 1 < s \\ C_{dec}[S-(1-s)S_{ref}], & \frac{S}{S_{ref}} < (1-s) \end{cases} \tag{24}$$

On these equations, S is the mechanobiological stimulus to bone apposition, that we compute as:

$$S = \sum_i (n_i \overline{\sigma}_i^m)^{1/m}, \tag{25}$$

being $\overline{\sigma}_i$ the Von Mises stress due to the ith load, and n_i the corresponding number of cycles. m is an empirical factor set to $m = 4$. As default case, parameters S_{ref}, s, C_{in} and C_{dec} were given values of 60 MPa, 0.6, 2×10^{-3} mm/day and 5×10^{-3} mm/day respectively. Bone apposition rate $\dot{r}$ was limited by the inequality -4×10^{-3} mm/day $\leq \dot{r} \leq 4 \times 10^{-3}$ mm/day .

To compute bone density, appositional bone density ρ_a is considered equivalent to cortical bone density $\rho_c = 1.75$ g/cm^3. Minimum bone density was considered to be $\rho_t = 0.1$ g/cm^3. Bone internal remodeling velocity was computed as:

$$\dot{\rho} = S_v(\rho)\rho_c \dot{r}, \tag{26}$$

by using the correlation due to Martin [38] for $S_v(\rho)$,

$$\begin{aligned} S_v(\rho) &= (\frac{\rho}{\rho_c})^2(0.07 + 8.1 \times 10^{-6}\rho - 7.2 \times 10^{-12}\rho^2 \\ &+ 5.1 \times 10^{-18}\rho^3 - 2.1 \times 10^{-24}\rho^4 + \\ &+ 0.23 \times 10^{-30}\rho^5), \end{aligned}$$

for $[\rho] = \frac{\text{g}}{\text{cm}^3}$.

Mechanical properties:. Model regions are considered as Hookean, isotropic materials as default. Poisson ratio of elements in Ω_B is given the value $\nu = 0.3$, while the value $\nu = 0.45$ is adopted for elements in Ω_F. Young modulus is considered to be constant and equal to 20 MPa for the elements in Ω_F, while for

the elements in Ω_B the correlation

$$E(\rho)[\text{MPa}] = \begin{cases} 2018\rho^{2.5} & 0.1 < \rho \leq 1.2 \\ 1744\rho^{3.3} & 1.2 < \rho \leq 1.75 \end{cases}, \tag{27}$$

for $[\rho] = [\frac{\text{g}}{\text{cm}^3}]$ was applied.

3.2. Case 1: Hemiepiphysiodesis treatment

In this section, we use the formulated algorithm to explore the problem of bone growth for a simplified 2D model of the distal femur during epiphyseal stapling. Such treatment is an alternative when significant differences occur in the growth speed of different regions within the same epiphyseal plate. This results in an angular deviation of the affected long bone, that can be assessed, if the epiphyseal plate remains open, by inserting a Blount staple in the more rapidly growing side of the physis, thus restraining growth until the initial angular deviation is corrected [13, 39]. This particular scenario is characterized by the interaction between all the considered phenomena, given by the presence of an orthotic device interacting with longitudinal growth and bone remodeling.

Consider a section of the distal femur, as shown in Fig. 3, which we study under the hypothesis of a plane deformations stress state. This section was obtained after sectioning along the coronal plane and scaling by a factor of 0.75 the Standardized Femur [34] in order to reflect the geometry of a child bone. It must be emphasized here that the shown results are oriented towards algorithm validation, thus limitations exist regarding geometry accuracy. Used mesh and code are provided in Supplementary Material 1.

A set of loads (F_L,F_M) acts on the lateral and medial epichondyles of the bone respectively, which define $\partial\Omega_N$. Nodal displacements are blocked on the proximal boundary of the model, $\partial\Omega_D$, Fig. 3. A region Ω_P, with a Young modulus of 210 MPa and a Poisson ratio of 0.3, representing an inserted titanium Blount staple was defined.

Initial density is obtained after considering a 'non-stapled' model, for which only the remodeling algorithm is applied until the convergence criterium $\max[\rho(t+$

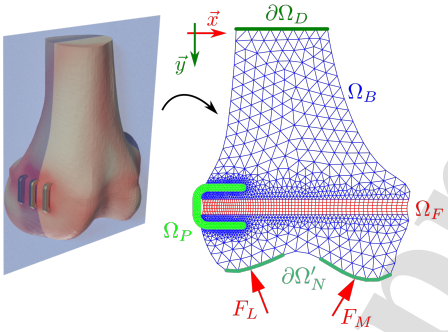

Load case	F_L[N/mm]	F_M[N/mm]	n
1	15	15	6000
2	0	7.5	3000
3	7.5	0	3000

Figure 3: 2D modeling of the growth in the distal femur under an hemiepiphysiodesis treatment. Forces directions were obtained by integration of an uniform pressure distribution on the considered epichondyle.

$\Delta t) - \rho(t)] \leq 1 \times 10^{-8} \frac{\mathrm{g}}{\mathrm{cm}^3}$ is achieved. A stress free initial condition is established. Obtained density is projected into an 'stapled' model, upon which growth simulation proceeds.

Upper line in Fig. 4 shows the evolution of bone density for a time lapse of 100 days. Initial geometry is shown with a black contour. On this line, Detail A shows the computed bone apposition for this case. Detail B shows the advance of the physeal ossified zone, while detail C shows the computed longitudinal growth. In the lower line of Fig. 4 it is possible to observe the evolution of the growth direction coincident stress tensor component. This particular variable can be interpreted as the stress pressure, as defined by some authors [39]. It is worth noticing here that not only a compressive load appears in the zone between the staple legs, but also a tensile load appears on the diaphyseal zone next to the staple. A reduction in the epiphyseal thickness can be identified on this zone, showing how it would be also possible to predict the risk of physeal

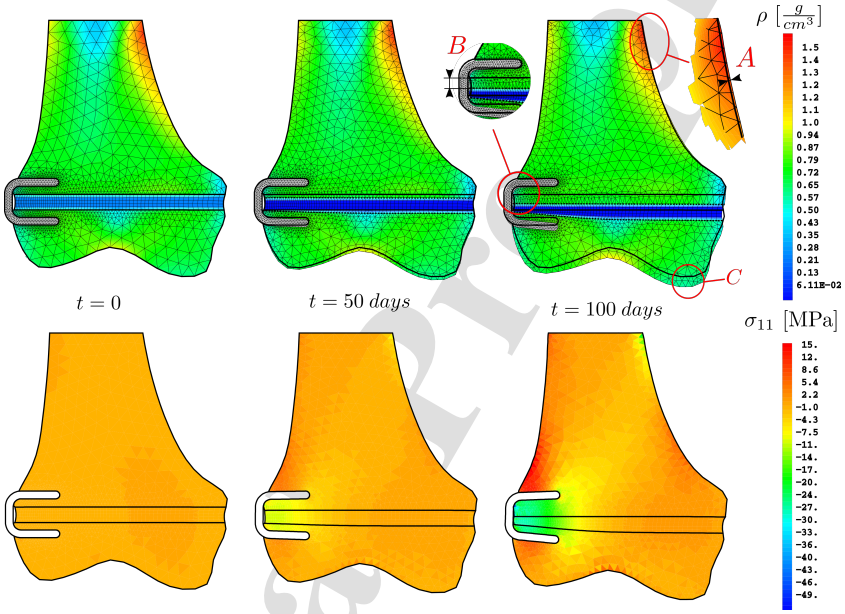

Figure 4: Growth relevant results. Upper line shows bone shape and density evolution, while lower line shows the computed growth pressure (i. e., the pressure exerted by growth in order to accommodate to the presence of a permanent device). Detail A shows external remodeling in the proximal portion of the diaphysis. Detail B shows computed advance in ossification front. Detail C shows changes in shape due both to growth and bone remodeling.

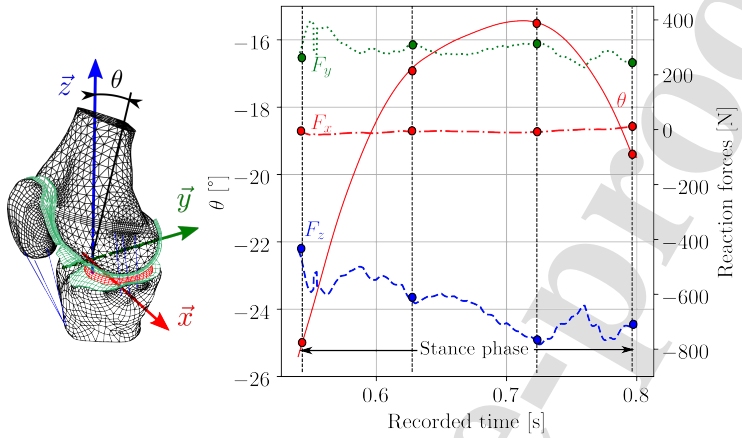

Figure 5: Load states considered for the evaluation of mechanobiological growth in the distal femur. Plotted forces correspond to the reaction forces on the knee obtained from gait analysis, while the dots indicate the considered points of the stance phase. For further reference, refer to Supplementary Material N° 2.

closure.

3.3. Case 2: Growth in the distal femur

In this section, we show the manner in which biomechanical data can be integrated into the proposed algorithm to consider the mechanobiological effect of a pathological gait pattern on longitudinal growth. For this, data experimentally obtained for a patient with crouch gait (*Case_02_model,* reported by Steele et al. [40]) are incorporated into a 3D contact model of the knee. Considered loads were those due to the gastrocnemius, the vastus, and the rectus femoris, as well as the knee reaction forces. For further details about the geometrical model, material properties and boundary conditions used to compute contact loads please refer to Supplementary Material N° 2.

Four load states are considered, corresponding to the 0%, 33%, 66% and 100% of the stance phase (Fig. 5). Each of this loads was assigned a number of cycles of 200.

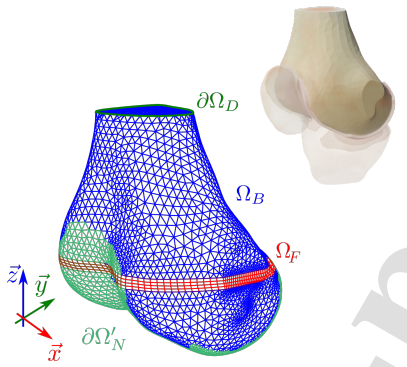

Figure 6: Modeling of bone growth in the distal femur. Loads on the model are obtained from a 3D finite elements contact model.

The 3D contact model of the knee was reduced to consider only the femur. Then, the nodal forces computed from the contact model were projected into the femoral interface with the articular cartilage and the ligaments, which define the Neumann boundary $\partial\Omega_N$. Nodal displacements are blocked in the proximal border of the model, $\partial\Omega_D$, Fig. 6.

We characterize deviations from normal growth, in terms of the displacement speed $\dot{u}$ of a given point r, on the interface of the physis and the epiphysis, for $t \to 0$. In order to simplify the analysis, we define a rotation center $\vec{r}^{\mathbf{c}}$, as the point that satisfies the condition:

$$\int_A \dot{u} \times \vec{r}^{\mathbf{c}} dA = \int_A \dot{u} \times \vec{r} dA, \tag{28}$$

being dA a differential surface element. We also define a mean rotation speed $\vec{\psi}$ about the x, y and z axis respectively, as:

$$\begin{cases} \psi_x &= \frac{1}{A}\int_A \dot{u}_z(y - r_y^c)dA \\ \psi_y &= \frac{1}{A}\int_A \dot{u}_z(x - r_x^c)dA \\ \psi_z &= \frac{1}{A}\int_A [\dot{u}_y(x - r_x^c) + \dot{u}_x(y - r_y^c)]dA \end{cases} \tag{29}$$

Notice that, in terms of the adopted coordinate system, Fig. 5, rotation speed components represent the recurvatum, valgus/varus and anteversion deviation speeds of the joint respectively.

Fig 7 shows a set of relevant results. In Fig. 7a, equilibrium bone density is shown. A high density zone is computed for the cortical zone of the model, which is consistent with the normal bone structure. Bone is shown to strengthen in the medial zone, as compared with the lateral side. Fig. 7 shows the longitudinal growth speed. A speed decrease is observed in the lateral side of the epiphyseal plate, as compared with the growth speed in the medial side. As a result, a mean rotation speed of $\vec{\psi} = (-2.48 \times 10^{-5}, -4.47 \times 10^{-4}, -1.08 \times 10^{-5})$ day^{-1} can be calculated. This results could equivalently be interpreted as the induction of a recurvatum, a varus and an anteversion rotation deformation at a rate of $0.52, 9.3$ and 0.23 degrees per year induced by crouch gait. As it can be inferred from the pressure distribution in the femoral cartilage (Supplementary material N° 2), crouch gait results in an increased load in the medial epichondyle. Consistently, this leads to an increased bone density on this side of the bone, as well as a decreased growth speed, deriving in a predominantly genu varum deformity.

3.4. Case 3: Bone remodeling around hip prosthesis

Proposed algorithm reduces to the classical approach initially taken by Beaupré et al. [6] when no growth is considered (i. e., $\Omega_F = \phi$). To illustrate a typical case, we consider bone remodeling around a hip prosthesis, Fig. 8. Relevance of this problem is due to the presence of a phenomenon called stress shielding. It is characterized by a density diminishment in the vicinity of an inserted orthotic, associated with a load transfer from the bone to the device, that results in bone resorption and can lead to loosening or failure of the device [15, 41].

To study a real-like situation, we consider the domain shown in Fig. 8. Considered loads are taken from the work by Garijo et al. [42], and they correspond to the forces exerted by the gluteus maximus muscle (F_G) and the hip reaction (F_H).

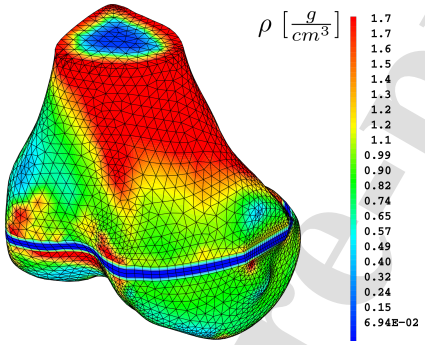

(a) Estimated distal femur density.

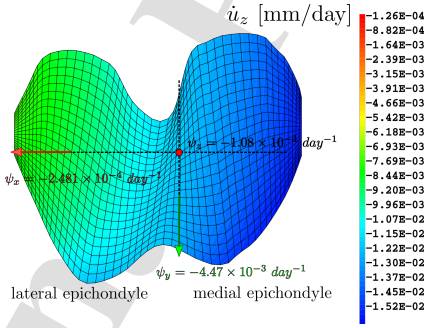

(b) Longitudinal growth speed in the distal femur. Red dot shows the rotation center of the load-induced deformity.

Figure 7: Density and longitudinal growth characterization of the distal femur.

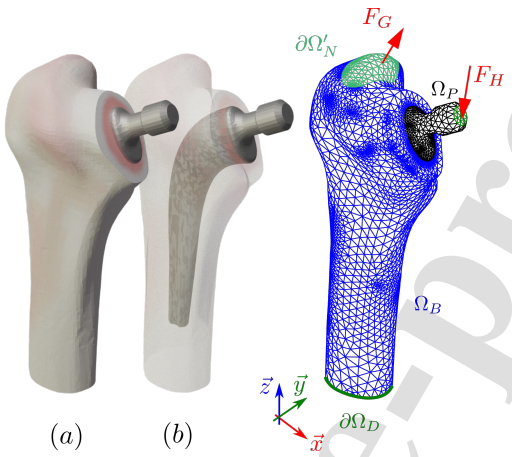

Figure 8: 3D modeling of bone remodeling around hip prosthesis (a). A titanium prosthesis is inserted into the proximal portion of the femur (b). Loads representing the gluteus maximus muscle force F_G and the hip reaction F_H are applied, according with [42].

Proposed algorithm allows to calculate the stationary bone density distribution of the femur, as shown in Fig. 9. Left image shows the external local density distribution, while the right image shows the local density along the symmetry plane of the prosthesis. Performed calculations allow to infer that the insertion of a hip prosthesis leads to an increased thickness of the cortical region in the zone surrounding the distal portion of the device, while a bone density diminishment is observed in the proximal portion of the femur.

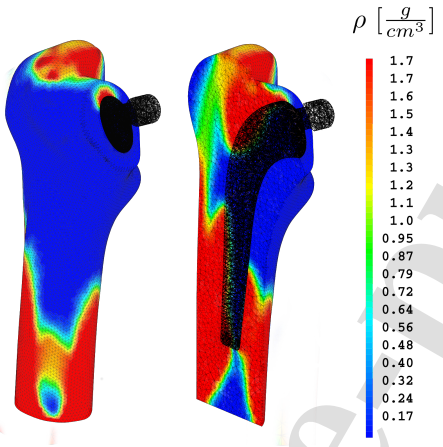

Figure 9: Bone density distribution around hip prosthesis.

Conclusions

A new tool for solving bone growth and remodeling problems, characterized by the presence of a time-dependent domain was developed. A generalized mathematical formulation of these was established. A finite elements algorithm, relying in the application of a prescribed displacement to the nodes of the used mesh, together with an explicit time-integration scheme was proposed for its resolution.

As opposed to currently applied methods, in which the bone regions are tracked by identifying the elements of the domain that are susceptible to grow, the methodology proposed here allows to drastically increase the accuracy of the evaluated geometrical changes, to date limited by the size of the used mesh elements. For bone growth problems, the generated displacements depend on the integral of the growth tensor in the whole domain (Eq. 11). This mathematical feature is a key difference between these problems and classical fluid or solids mechanics problems, in which particles displacements and speed depends

fundamentally on the forces exerted over differential mass points. On the cases studied here, when trying to apply conventional methods as immersed FEM and/or CutFEM for solving growth problems, unless very fine and computationally expensive meshes are used, errors in computed growth for an interior point of the domain are integrated causing severely large errors in the computed displacement of the points in the boundary of it.

A set of classical bone growth and remodeling equations was chosen to demonstrate the applicability of the proposed algorithm. It is worth noticing that the main target of this work was to analyze the suitability of the proposed methodology, rather than the study of model specific results. It was used to predict changes in bone morphology due to bone apposition, as well as bone longitudinal growth. It was also found to be adequate for computing bone local density changes. The feasibility of integrating biomechanical data to compute bone growth deformities development was demonstrated, as well as the feasibility of computing internal stresses in the bone due to the interaction of longitudinal growth with orthotic devices.

Our algorithm has been incorporated in a Cast3M library, that has been provided as a supplementary material. This library, as well as a set of eight implementation examples provided along, constitute what we believe could be a valuable tool for research purposes.

Funding

Authors acknowledge funding from CNEA and projects SIIP UNCuyo 06/045 (2019-2021) and ANPCyT PICT 2018-03300.

References

[1] Carter D, Beaupré G. Skeletal function and form. Mechanobiology of skeletal development, aging and regeneration. Cambridge University Press; 2001. ISBN 0 521 79000 X (hb).

[2] Pous JG, Dimeglio A, Baldet P, Bonnel F. Cartilage de conjugaison et croissance. Notions fondamentales en orthopédie; vol. 28. Doin éditeurs; 1980. ISBN 2-7040-0359-9.

[3] Stevens SS, Beaupré GS, Carter D. Computer model of endochondral growth and ossification in long bones. biological and mechanobiological influences. Journal of orthopaedic research 1999;17:646–53.

[4] Bonnel F, Dimeglio A, Baldet P, Rabischong P. Biomechanical activity of the growth plate. Clinical Anatomy 1984;6:53–61.

[5] Roesler H. The history of some fundamental concepts in bone biomechanics. Journal of Biomechanics 1987;20(11-12):1025–34. doi:10.1016/0021-9290(87)90020-0.

[6] Beaupré GS, Orr TE, Carter DR. An approach for time-dependent bone modeling and remodeling. theoretical development. Journal of orthopaedic research 1990;8:651–61.

[7] Mikic B. Epigenetic influences on long bone growth, development, and evolution. UMI; 1996.

[8] Mikic B, Clark RT, Battaglia TC, Gaschen V, Hunziker EB. Altered hypertrophic chondrocyte kinetics in gdf-5 deficient murine tibial growth plate. Journal of orthopaedic research 2004;22:552–6.

[9] Hambli R. Connecting mechanics and bone cell activities in the bone remodeling process: an integrated finite element modeling. The Journal of Arthroplasty 2014;5:191–200.

[10] Marsik F, Klita V, Chlup H. Remodelling of livin bone induced by dynamic loading and drug delivery - numerical modelling and clinical treatment. Mathematics and Computers in Simulation 2010;80:1278–88.

[11] Ueki M, Tanaka N, Tanimoto K, Nishio C, Honda K, Lin YY, et al. The effect of mechanical loading on the metabolism of growth plate chondro-

cytes. Annals of Biomedical Engineering 2008;36(5):793–800. doi:10.1007/s10439-008-9462-7.

[12] Giorgi M, Carriero A, Shefelbine S, Nowlan N. Effects of normal and abnormal loading conditions on morphogenesis of the prenatal hip joint: application to hip dysplasia. Journal of Biomechanics 2015;48:3390–7.

[13] Peterson HA. Physeal injury other than fracture. Springer, London; 2012. ISBN 978-3-642-22563-5.

[14] Phillips A, Villette C, Modenese L. Femoral bone mesoscale structural architecture prediction using musculoskeletal and finite element modelling. 2015;2:43–61.

[15] Orr TE, Beaupré GSea. Computer predictions of bone remodeling around porous-coated implants. The Journal of Arthroplasty 1990;5:191–200.

[16] Cheong VS, Blunn GW, Coathup MJ, Fromme P. A novel adaptive algorithm for 3d finite element analysis to model extracortical bone growth. Computer methods in biomechanics and biomedical engineering 2018;.

[17] Carter DR, Wong M. The role of mechanical loading histories in the development of diarthrodial joints. Journal of Orthopaedic Research 1988;6:804–16.

[18] Stokes IA, Laible JP. Three-dimensional osseo-ligamentous model of the thorax representing initiation of scoliosis by assymetric growth. J Biomechanics 1989;23:589–95.

[19] Carter DR, Van Der Meulen MCH, Beaupré GS. Mechanical factors in bone growth and development. Bone 1996;18:5S–10S.

[20] Sylvestre P, Villemure I, Aubin CE. Finite element modeling of the growth plate in a detailed spine model. Medical and Biological Engineering and Computing 2007;45:977–88.

[21] Giorgi M, Carriero A, Shefelbine S, Nowlan N. Mechanobiological simulations of prenatal joint morphogenesis. Journal of Biomechanics 2014;47:989–95.

[22] Yadav P, Shefelbine S, Gutierrez-Farewick EM. Effect of growth plate geometry and growth direction on prediction of proximal femoral morphology. Journal of Biomechanics 2016;.

[23] Goda I, Ganghoffer JF, Maurice G. Combined bone internal and external remodeling based on eshelby stress. International Journal of Solids and Structures 2016;doi:10.1016/j.ijsolstr.2016.04.036.

[24] Lin H, Aubin C, Parent S, Villemure I. Mechanobiological bone growth: comparative analysis of two biomechanical modelling approaches. Medical and Biological Engineering and Computing 2009;47:357–66.

[25] Carriero A, Jonkers I, Shefelbine S. Mechanobiological prediction of proximal femoral deformities in children with cerebral palsy. Computer methods in biomechanics and biomedical engineering 2011;14(3):253–62.

[26] Beaupré GS, Orr TE, Carter DR. An approach for time-dependent bone modeling and remodeling. application: A preliminary remodeling simulation. Journal of orthopaedic research 1990;8:662–70.

[27] Kaviani R, Londono I, Parent S, Moldovan F, Villemure I. Growth plate cartilage shows different strain patterns in response to static versus dynamic mechanical modulation. Biomech Model Mechanobiol 2015;.

[28] Anderson M, Green W, Messner M. Growth and predictions of growth in the lower extremities. The Journal of Bone and Joint Surgery 1963;45:1–14.

[29] Hunziker E. Mechanism of longitudinal bone growth and its regulation by growth plate chondrocites. Microscopy research and technique 1994;28:505–19.

[30] Rozbruch SR, Ilizarov S. Limb lenghthening and reconstruction surgery. Informa healthcare, New York; 2007. ISBN 978-0-8493-4051-2.

[31] Alonso M, Bertolino G, Yawny A. Mechanobiological based long bone growth model for the design of limb deformities correction devices. Journal of Biomechanics 2020;109:109–905. URL: https://doi.org/10.1016/j.jbiomech.2020.109905. doi:10.1016/j.jbiomech.2020.109905.

[32] Xinghua Z, He G, Bingzhao G. The application of topology optimization on the quantitative description of the external shape of bone structure. Journal of biomechanics 2005;38:1612–20.

[33] CEA . Cast3m v20.0.1. http://www-cast3m.cea.fr/index.php; 2020.

[34] The bel repository. http://www.tecno.ior.it/VRLAB/; 2016.

[35] Wangerin S. Cal poly human motion biomechanics lab knee joint finite element model. https://simtk.org/projects/cphmbkneefem/; 2020.

[36] platform S. Salome-mesh v9.2. http://www.salome-platform.org/; 2020.

[37] Meng Y, Untaroiu CD. A review of pediatric lower extremity data for pedestrian numerical modeling: Injury epidemiology, anatomy, anthropometry, structural, and mechanical properties. Applied Bionics and Biomechanics 2018;2018.

[38] Martin R. Porosity and specific surface of bone. Critical Reviews in Biomedical Engineering 1984;:179–222.

[39] Bylski-Austrow DI, Wall EJ, Rupert MP, Roy DR, Crawford AH. Growth plate forces in the adolescent human knee: A radiographic and mechanical study of epiphyseal staples. Journal of Pediatric Orthopaedics 2001;21(6):817–23. URL: https://doi.org/10.1097/01241398-200111000-00023. doi:10.1097/01241398-200111000-00023.

[40] Steele K, Seth A, Hicks JL, Schwartz MS, Delp SL. Muscle contributions to support and progression during single-limb stance in crouch gait. Journal of Biomechanics 2010;43:2099–105.

[41] Yuehuei H, Draughn RA. Mechanical testing of bone and the bone implant interface. CRC Press; 2000.

[42] Garijo N, Fernández JR, Pérez MA, García-Aznar JM. Numerical stability and convergence analysis of bone remodeling model. Comput Methods Appl Mech Engrg 2014;271:253–68.

A novel algorithm is proposed for solving bone growth and ossification problems, and its interaction with prosthetic devices.

A significant reduction in errors and computational costs as compared with previously taken approaches is achieved.

An open source package is provided.

A set of eight scripts with implementation/validation examples is provided.

Relevant studied cases comprise bone growth and remodeling for hemiepiphysiodesis treatments,
bone remodeling around hip prosthetics and bone growth and remodeling in the pediatric knee.

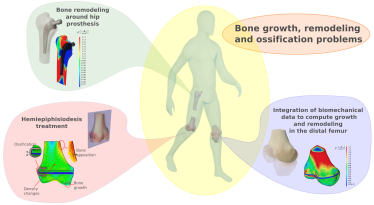
Bone remodeling around hip prosthesis
Bone growth, remodeling and ossification problems
Hemiepiphisiodesis treatment
Integration of biomechanical data to compute growth and remodeling in the distal femur

AUTHOR STATEMENT

Gastón Alonso: Conceptualization; Investigation; Methodology; Software; Validation; Visualization; Roles/Writing - original draft; Writing - review & editing.

Alejandro Yawny: Formal analysis; Funding acquisition; Project administration; Resources; Supervision; Writing - review & editing.

Graciela Bertolino: Conceptualization; Formal analysis; Funding acquisition; Investigation;Project administration; Resources; Supervision; Writing - review & editing.

Declaration of interests

☒ The authors declare that they have no known competing financial interests or personal relationships that could have appeared to influence the work reported in this paper.

☐ The authors declare the following financial interests/personal relationships which may be considered as potential competing interests: